

Rolling vs. Seasonal PMF: Real-world multi-site and synthetic dataset comparison

Marta_Via^{1,2}, Gang Chen³, Francesco Canonaco^{3,4}, Kaspar R. Daellenbach³, Benjamin Chazeau⁵, Hasna Chebaicheb^{6,7}, Jianhui Jiang⁸, Hannes Keernik^{9,10}, Chunhui Lin¹¹, Nicolas Marchand⁵, Cristina Marin^{12,13}, Colin O'Dowd¹¹, Jurgita Ovadnevaite¹¹, Jean-Eudes Petit¹⁴, Michael Pikridas¹⁵, Véronique Riffault⁶, Jean Sciare¹⁵, Jay G. Slowik³, Leila Simon^{7,13}, Jeni Vasilescu¹², Yunjiang. Zhang^{7,13}, Olivier Favez⁷, André S. H. Prévôt³, Andrés Alastuey¹, María Cruz Minguillón¹

¹Institute of Environmental Assessment and Water Research, Barcelona, 08034, Spain

²Department of Applied Physics, University of Barcelona, Barcelona, 08028, Spain

³Laboratory of Atmospheric Chemistry, Paul Scherrer Institute, CH-5232 Villigen PSI, Switzerland

⁴Datalystica Ltd., Park innovAARE, 5234 Villigen, Switzerland

⁵Aix Marseille Univ., CNRS, LCE, Marseille, France

⁶IMT Nord Europe, Institut Mines-Télécom, Univ. Lille, Centre for Energy and Environment, 59000 Lille, France

⁷Institut National de l'Environnement Industriel et des Risques, Parc Technologique ALATA, 60550, Verneuil-en-Halatte, France

⁸Shanghai Key Lab for Urban Ecological Processes and Eco-Restoration, School of Ecological and Environmental Sciences, East China Normal University, 200241 Shanghai, China

⁹Air Quality and Climate Department, Estonian Environmental Research Centre, Marja 4d, 10617 Tallinn, Estonia

¹⁰Department of Software Science, Tallinn University of Technology, 19086 Tallinn, Estonia

¹¹School of Physics and Centre for Climate and Air Pollution Studies, Ryan Institute, National University of Ireland Galway, University Road, H91CF50 Galway, Ireland

¹²National Institute of Research and Development for Optoelectronics INOE2000, Atomistilor 409, RO77125 Magurele, Romania

¹³Department of Physics, Politehnica University of Bucharest, 313 Spl. Independentei Str., Bucuresti, Romania

¹⁴Laboratoire des Sciences du Climat et de l'Environnement, Orme des Merisiers, 91190 Gif-sur-Yvette, France

¹⁵Climate and Atmosphere Research Center, The Cyprus Institute, Nicosia, 2121, Cyprus

Correspondence to: Marta Via (marta.via@idaea.csic.es)

Abstract.

Particulate Matter (PM) has become a major concern in terms of human health and climate impact. In particular, the source apportionment (SA) of organic aerosols (OA) present in submicron particles (PM_{10}) has gained relevance as an atmospheric research field due to the diversity and complexity of its primary sources and secondary formation processes. Moreover, relatively simple but robust instruments such as the Aerosol Chemical Speciation Monitor (ACSM) are now widely available for the near real-time online determination of the composition of the non-refractory PM_{10} . One of the most used tools for SA purposes is the source-receptor Positive Matrix Factorization (PMF) model. Even though the recently developed *rolling PMF* technique has already been used for OA SA on ACSM datasets, no study has assessed its added value compared to the more common seasonal PMF method from a practical approach yet. In this paper, both techniques were applied to a synthetic dataset and to nine European ACSM datasets in order to spot the main output discrepancies between methods. The main advantage of the synthetic dataset approach was that the methods' outputs could be compared to the expected 'true' values, i.e. the original synthetic dataset values. This approach revealed similar apportionment results amongst methods, although the *rolling PMF* profile adaptability feature has been proven advantageous as it generated output profiles moving nearer to the truth points. Nevertheless, these results highlighted the impact of the profile anchor on the solution, as the use of a different anchor with respect to the truth led to significantly different results in both methods. In

Eliminado: concerning

Eliminado: but differing with respect to the truth,

Eliminado:

Eliminado: Also

the multi-site study, while differences were generally not significant when considering year-long periods, their importance grew towards shorter time spans, as in intra-month or intra-day cycles. *Rolling* PMF performed better than *seasonal* PMF globally for the ambient datasets investigated here as far correlation with external measurements is concerned, especially in periods between seasons. The results of this multi-site comparison coincide with the synthetic dataset in terms of *rolling-seasonal* similarity and *rolling* PMF reporting moderate improvements. Altogether, the results of this study provide solid evidence of the robustness of both methods and on the overall efficiency of the recently-proposed *rolling* PMF approach.

Eliminado: also support *rolling* PMF benefits even though output discrepancies with *seasonal* PMF were scarce

Con formato: Fuente: Cursiva

Con formato: Fuente: Cursiva

1 Introduction

Air pollution is one of the biggest current and future environmental threats to human health and climate change. Results from Chen and Hoek, (2020) notably relate an increased risk for all-cause mortality due to fine aerosol (PM_{2.5}, particulate matter of aerodynamic particle diameter below 2.5 micrometres) exposure. Also, even for concentrations below the WHO guidelines threshold (annual means of 10 µg·m⁻³ for PM_{2.5} at the time that article was published), the life expectancy of the population of Europe has been reduced by about 8.6 months on average. In turn, fine atmospheric aerosols also play a role in climate change (IPCC, 2021) due to both their direct (through radiation) and indirect (through cloud interaction) effects.

Exposure to submicron particulate matter (PM₁, particulate matter with an aerodynamic particle diameter less than 1 µm) is known to have severe impacts on the respiratory system (Yang et al., 2018), and even pass the blood-brain barrier to act directly on the central nervous system (Shih et al., 2018; Yin et al., 2020). Impact mitigation strategies must be designed to both reduce emissions (primary aerosols) and prevent the formation of non-directly-emitted (or secondary) aerosols, but also target the most harmful components, especially since recent studies have demonstrated the mitigation strategies might be more effective in tackling specific PM sources rather than the bulk PM (Daellenbach et al., 2020). With the purpose of identifying the most appropriate reduction strategies, source apportionment (SA) methodologies, designed for identifying pollutant sources, must be constantly improved. One of the most widely used receptor models for SA is the Positive Matrix Factorization (PMF) model (Paatero and Tapper, 1994) along with the ME-2 engine (Paatero, 1999). This model can handle various types of data, such as online and offline PM datasets (Amato et al., 2016; Crippa et al., 2014; Rai et al., 2020, respectively), VOCs (Yuan et al., 2012), multi-wavelength absorption of refractory carbon (Forello et al., 2019) etc.; assemble different types of pollutants (Ogulei et al., 2005); and also be coupled to machine learning techniques (Heikkinen et al., 2020; Rutherford et al., 2021).

Since organic species account for 20–90% of the total submicron aerosol mass (Chen et al., 2022; Jimenez et al., 2009) scientific interest has been set on the characterization of these pollutants by offline and online techniques. The use of ACSM (Aerosol Chemical Speciation Monitor, Aerodyne Research Inc., Billerica, MA, USA) for continuous monitoring and quantification of submicron non-refractory compounds has become a key approach for air quality (AQ) assessment. The application of PMF to long-term ACSM submicron organic aerosol (OA) datasets (Sun et al., 2018; Zhang et al., 2019) under the Source Finder (SoFi) Pro software package (Datalystica Ltd.) allows to quantify and identify the contribution of major groups of organic compounds. The formerly recommended methodology for OA SA was *seasonal* PMF, which requires splitting the dataset into seasons to

perform PMF independently, providing *seasonal* but not an intra-seasonal variation of factor profiles, as reported in Canonaco et al. (2015). The more recently developed *rolling* PMF (Canonaco et al., 2021; Parworth et al., 2015) applies the model on moving/rolling windows of a selected length and therefore it accounts for the temporal evolution of the OA source fingerprints. The current state-of-the-art supports that *rolling* PMF should be more accurate and/or suitable than *seasonal* PMF due to its profile-adaptation feature, and lower computational and evaluation time, which will be the base hypothesis of this study. Nevertheless, only a few individual studies (Chazeau et al., submitted; Chen et al., 2020; Tobler et al., 2021) and an intercomparison (Chen et al., 2022) have been published so far with this technique and no thorough *seasonal* vs. *rolling* comparison has been conducted thus far to the best of our knowledge.

This research aims to contribute to a deeper understanding of the advantages and weaknesses of the *rolling* and *seasonal* methods, assessing the differences regarding site or dataset characteristics and evaluating the environmental reasonability of their outcomes. This task is of great importance as the knowledge of the strengths of each method will come in handy to choose the best one for each study necessity, e.g., the better SA method for specific OA sources outbreaks. Furthermore, conclusions from this analysis will also impact the quality of health, climate and modelling studies by means of an improved description of the main OA pollution sources.

2 Methodology

2.1 Instrumentation and datasets.

This study is one of the outcomes of the Chemical On-Line cOmpoSition and Source Apportionment of fine aerosol (COLOSSAL) project (<https://www.costcolossal.eu/>) supported by the COST programme, and based on measurements performed within the ACTRIS network. It is closely related to the overview study of Chen et al. (2022), in which 22 more than one-year-long PMF datasets were joined for a *rolling* PMF intercomparison. Participants of the WG2 of the COST COLOSSAL Action contributed to the preparation of a protocol for SA with the purpose of homogenization of the PMF application (Chen et al., 2022). Nine of the 22 datasets from that study, whose main characteristics can be found in Table 1, were also provided for this *rolling-seasonal* comparison. Some of them contain site-specific sources related to instrument artefacts or proximity to pollution hotspots. The factors identified at all sites are Hydrocarbon-like OA (HOA), Biomass Burning OA (BBOA, except for the Dublin site), Less-Oxidised Oxygenated OA (LO-OOA), More-Oxidised Oxygenated OA (MO-OOA) and Oxygenated OA (OOA), which represents the sum of LO-OOA and MO-OOA. Other factors are only present at one or two sites: Cooking-Like OA (COA; in Barcelona-Palau Reial and Marseille-Longchamp), 58-related OA (58-OA; in Magadino), Shipping and Industry OA (SHINDOA; in Marseille-Longchamp), Wood Combustion, Coal Combustion and Peat Combustion OA (WCOA, CCOA, PCOA respectively; in Dublin). The 58-related OA, as explained in Chen et al. (2021), is a factor dominated by nitrogen fragments (m/z 58, m/z 84, m/z 94) which appeared as an artefact after the filament replacement in that instrument.

All data presented in the multi-site intercomparison were obtained from ACSMs, which use a mass spectrometer to measure the composition of non-refractory submicron particulate matter (NR-PM₁) in near real-time. It works

Eliminado: s, o their influence in results can be contrasted to sites with only more common sources.

Código de campo cambiado

Eliminado: (

Eliminado: ,

126 at a lower mass-to-charge resolution but it is more robust ~~compared to~~ the Aerosol Mass Spectrometer (AMS,
 127 Aerodyne Research Inc, Billerica, MA, USA) allowing for long-term deployment. Both quadrupole (Q-ACSM)
 128 and Time-of-Flight (ToF-ACSM) ACSMs were used, further described respectively in Fröhlich et al. (2013), Ng
 129 et al. (2011). The resolution of ToF-ACSM datasets (10 minutes) was averaged to 30 minutes (resolution of the
 130 Q-ACSM) to have ~~harmonised timestamps~~. The analysis software (version 1.6.1.1 for Q-ACSM and version 2.3.9
 131 for ToF-ACSM), implemented in Igor Pro (WaveMetrics, Inc.), was provided by Aerodyne Research Inc. The
 132 treatment of the multi-site ACSM data to generate PMF input matrices is summarised in SI Table S1 and more
 133 details can be found in the publications cited therein.

134 Ancillary measurements consisted of i. SO_4^{2-} , NO_3^- , NH_4^+ and Cl^- measurements from ACSM; ii. Black Carbon
 135 (BC) from filter-based absorption photometer AE33 from Magee Scientific (Drinovec et al., 2015), except for
 136 Cyprus Atmospheric Observatory – Agia Marina and Magadino, in which the AE31 was used. BC concentrations
 137 were differentiated according to their main sources, into fossil fuel (BC_{ff}) and wood burning (BC_{wb}) BC by
 138 applying the Sandradewi model (Sandradewi et al., 2008); iii. NO_x concentrations; iv. Ultra-fine particles (range
 139 20-1000 nm) at the Marseille - Longchamp site. Details on the complementary instrumentation at each site can be
 140 found in SI Table S2.

141 2.2 Synthetic dataset

142 Although the principal aim of this article is to inspect the differences in the methods amongst these European sites,
 143 firstly a synthetic dataset comparison was tackled. The main advantage of this procedure is that it allows mimicking
 144 real-world environmental measurements already classified in OA sources so that PMF results can be compared
 145 with the incoming synthetic data. We created a synthetic dataset that mimics OA mass spectral analyses of a ToF-
 146 ACSM in Zurich. For that purpose, we used source-specific OA mass spectra retrieved from the AMS Spectral
 147 database (Crippa et al., 2013; Ng et al., 2011b; Ulbrich et al., 2009) and OA source concentration time series
 148 generated by the air quality model CAMx (Comprehensive Air Quality Model with Extensions) previously
 149 published by Jiang et al. (2019). Details are described in the SI section A. ~~The dataset used to calculate the error~~
 150 ~~matrix is that from the Zurich site which ranges from February 2011 until December 2011. Hence, the same CAMx~~
 151 ~~outcoming time series period was used to generate the concentration matrix.~~ The represented OA sources are HOA,
 152 BBOA, SOA from biogenic emissions (SOA_{bio}), SOA from biomass burning (SOA_{bb}) and SOA from traffic and
 153 other anthropogenic sources (SOA_{tr}).

154 The first step for the synthetic dataset creation was to select p (number of factors), POA and SOA spectral profiles
 155 from the High-Resolution AMS Spectral database (Crippa et al., 2013; Ng et al., 2010; Ulbrich et al., 2009) and
 156 multiply them by the time series of the same sources from the model output. ~~The error matrix was generated~~
 157 ~~following the same steps as for real-world data and real-world parameters were used as detailed in SI. For this~~
 158 ~~purpose, the dataset used is that from the Zurich site which ranges from February 2011 until December 2011.~~
 159 ~~Hence, the same CAMx outcoming time series period was used to generate the concentration matrix.~~ Gaussian
 160 noise was subsequently added to the outcoming matrix. The resulting matrices were used as *rolling* and *seasonal*
 161 PMF ~~input~~. Before the comparison to original factors, ~~several~~ tests as in the multi-site comparison have been
 162 performed to check the quality of the output, ~~such as the mass closure test or the scaled residuals profile revision.~~

Eliminado: concerning

Eliminado: a

Eliminado: granularity of

Eliminado: The dataset used to calculate the error matrix is that from the Zurich site which ranges from February 2011 until December 2011.

Con formato: Fuente: Sin Cursiva

Eliminado:

Eliminado: The resulting matrices were summed up resulting in the data matrix.

Con formato: Fuente: Sin Cursiva

Eliminado:

Eliminado: inputs and the corresponding PMF results were compared to the input data

Eliminado: similar

Eliminado: .

Eliminado: Posteriorly, the synthetic measurements and error matrices were used as an input for both *rolling* and *seasonal* PMF.

Con formato: Fuente: Cursiva

2.3 Positive Matrix Factorization

The Positive Matrix Factorization model (Paatero and Tapper, 1994) describes the measured matrix \mathbf{X} of n timestamps and m variables as a product of two matrices, \mathbf{G} and \mathbf{F} , plus a residual matrix \mathbf{E} for a given number of factors p :

$$x_{ij} = \sum_{k=1}^p g_{ik} \cdot f_{kj} + e_{ij} \quad (1)$$

The matrices \mathbf{G} and \mathbf{F} can be randomly initialised with *a priori* information. The model then iterates until the quantity

$$Q = \sum_{i=1}^n \sum_{j=1}^m \left(\frac{e_{ij}}{\sigma_{ij}} \right)^2, \quad (2)$$

where σ_{ij} represents the uncertainties of the input matrix \mathbf{X} , is minimised with respect to all model variables.

The use of *a priori* information reduces the rotational ambiguity of the model, consisting of a degeneration of solutions associated with a given Q value (Canonaco et al., 2013), and it is usually done from the *a*-value approach. This consists of initialising \mathbf{F} (or \mathbf{G}) with reference profiles (or time series) and multiplying them by the percentage of variation a , $a \in [0,1]$, where 0 and 1 would represent total constraint and freedom, respectively. The Source Finder (SoFi Pro, versions 6.8 and 8.04, Datalystica Ltd., Villigen, Switzerland) applies this algorithm through the Multi-linear Engine 2 (ME-2) (Paatero, 1999) within the Igor Pro software environment (Wavemetrics, Inc., Portland, OR, USA). SoFi is also a powerful software package for preparing the rolling conditions for the input matrices prior to the PMF algorithm and post-processing the outcomes afterwards.

2.3.1 Seasonal PMF

In order to apply *seasonal* PMF, the input matrix is divided into season-long submatrices and PMF is applied independently, adjusting the number of necessary factors to the requirements of each subperiod. In order to reach an environmentally-reasonable local Q minimum, the implementation of constraints on Primary Organic Aerosol factors (POA), has been performed according to the COLOSSAL guidelines for source apportionment (COLOSSAL, COST Action CA16109, 2019) and the protocol from Chen et al. (2022). After unconstrained results exploration, which allowed for some marker identification, constraints based on the *a*-value approach were applied to primary OA factors. The systematic exploration of the *a*-value space has been performed for each season with the aim of determining the combination of *a*-values which maximises the correlations between factors and external correlations and represents an environmentally-reasonable OA explanation, hereafter referred to as the base case solution. The random *a*-value ranges and the reference profiles employed can be found in SI Table S1 and Table S3 a.

With respect to the synthetic dataset, the 11 months from 2011 data were split into three periods (and not four seasons to avoid running PMF over too short periods): February – May, June – August and September – December. The real-world Marseille dataset also used the co-located SO_2 time series to force an Industry + Shipping factor to

212 emerge as reported in previous studies (Bozzetti et al., 2017; El Haddad et al., 2013). The seasonal averaging of
213 the remaining runs were complemented by bootstrapping to estimate the statistical error of the solution.

214 Bootstrapping (Efron, 1979) the *seasonal* PMF input together with random *a*-value resampling allows for
215 statistical and rotational uncertainty assessment. The application of criteria-based selection, which will be deeply
216 explained in 2.3.2, was also used to discard those runs which do not comply with the user-defined standards. The
217 outcome of this technique consists of *p* (number of factors) mass spectra and time series including their uncertainty
218 assessment combined season-wise together to obtain period-long OA sources. This might lead to possible factor
219 discontinuity. Moreover, from this approach, source fingerprints are static throughout a whole season and cannot
220 adapt to OA processes of lifetimes below a meteorological season (i.e., 90 days), but can nevertheless evolve from
221 one season to another.

222 **2.3.2 Rolling PMF**

223 *Rolling* PMF runs the model on subsets of the input matrix with a user-defined (window) length in days. Then, the
224 window is shifted by a number of days (also chosen by the user) and PMF is applied again (Parworth et al., 2015).
225 Consequently, many PMF runs are performed in each window length period, so in the post-analysis, one can
226 automatically discard the runs that do not meet certain user-defined criteria (Canonaco et al., 2015). To select the
227 most environmentally-reasonable runs, the remaining solutions are averaged to generate the final solution, which
228 will be provided with statistical and rotational uncertainties based on random input resampling (bootstrap) and
229 random *a*-value resampling, respectively.

230 A length of 14 days and a shift of 1 day were used in the current study for the synthetic dataset and for 7 out of the
231 9 datasets, which is a good compromise between Q/Q_{exp} values and the percentage of modelled points as suggested
232 in Canonaco et al. (2021). Window lengths of 28 days were also assessed, but the correlations to ancillary
233 measurements deteriorated in most of the cases. Exceptions to this rule were the SIRTa and Tartu sites, for which
234 the 28-day window offered better correlations. These window lengths are consistent with the life cycle lengths of
235 atmospheric aerosols (Textor et al., 2006) and their outcomes do not differ significantly. The application of
236 constraints in PMF, as advised in the protocols, consists of setting random *a*-values within a reasonable range and
237 accepting only the runs that comply with the criteria. This procedure will lead to the selection of *a*-values which
238 induce more environmentally-reasonable solutions, whose average will provide the final number. In some cases,
239 the reference profiles used in *rolling* PMF are those from the *seasonal* solution, as the protocol is flexible regarding
240 this choice. However, this constraint can have an impact on the solution, and in order to identify its implications,
241 the profiles used in each case are detailed in Table S1, Table S3a.

242 A criteria-based selection was developed to automatically inspect the large number of PMF runs provided by the
243 *rolling* method (Canonaco et al., 2021). This consists of the application of certain criteria to be fulfilled by the
244 PMF outcoming factors. The acceptance/rejection of a run can be dictated by the thresholds retrieved from
245 bootstrapped *seasonal* solutions, or more advisably, from a double-tailed Welch's t-test hypothesis evaluation with
246 *p*-values (Chen et al., 2021) chosen by the user (not exceeding 0.05). This procedure allows for factor discontinuity,
247 as one can run PMF for two consecutive numbers of factors, and choose a certain criterion upon which to select

one more (or less) factor depending on the outbreak/vanishing of a factor marker. The list of criteria is specified in SI Table S3 b for the synthetic dataset and in the respective publications for each real-world site.

2.4 SA procedure and dataset homogenization

A method to compare source apportionment performance, analogous to Belis et al. (2015) while adjusted for our specificities, was developed in this study. The first step consisted of preliminary checks, in which the minimum requirements for solution acceptance must be satisfied, such as the mass closure and reasonability of profiles. Secondly, the characterization of discrepancies between methods was addressed in order to confirm the presence or absence of significant differences between *rolling* and *seasonal* PMF. The decision on which method is more suitable for certain dataset particularities was *a posteriori* based on the quantification of the performance goodness of both methods by means of correlation to external measurements and residual analysis. This flow process was applied to both the multi-site analysis and the synthetic dataset.

All the participants of the multi-site comparison applied the SA protocol to their own datasets, benefiting from the expertise in the previous OA SA studies at their sites. The analysis of differences between source contribution estimates by both methods was performed for each site individually and overall. The similarity of time series from one method to the other was assessed not only for each whole dataset but also in a 'rolling' fashion, that is to say, by calculating some metrics on windows of a given number of days with 1-day shifts between windows. This approach allowed for the identification of significant discrepancies between both approaches for the set PMF window lengths (14 days for *rolling*, 90 days for *seasonal*), a feature which was not evident in the whole long-term time series. It also enabled watching intra-daily differences, by setting period lengths of 1 day.

A detailed study of model residuals was also beneficial to quantify the accuracy of each technique performance. Scaled residuals represent the model error (e_{ij}) normalised by the uncertainty matrix (σ_{ij}):

$$\text{Scaled residuals}_{ij} = \frac{e_{ij}}{\sigma_{ij}} \quad (3)$$

and their ij sum has been reported in Paatero and Hopke (2003) to describe a unimodal histogram within a ± 3 range under good model performance conditions. The output Q quantity has both been compared in a raw and in a normalised way. This normalisation aims to deprive the impact of the degrees of freedom that normally depend on the input size and on the number of factors, computing hence the quantity Q/Q_{exp} , where

$$Q_{exp} = m \cdot n - p \cdot (m + n) \quad (4)$$

Then, various PMF runs can be compared in a more fundamental way. The expressions used for the normalisation arrangement have to be adapted to the particular degrees of freedom of each method:

$$\left(\frac{Q}{Q_{exp}} \right)_{Rolling} = \frac{Q}{m \cdot n - p \cdot (n + m \cdot n_{14})} \quad (5)$$

$$\left(\frac{Q}{Q_{exp}} \right)_{Seasonal} = \frac{Q}{m \cdot n - p \cdot (n + m \cdot n_{90})} \quad (6)$$

279 The parameters $n_{14\text{ days}}$ and $n_{90\text{ days}}$ refer to the number of periods throughout the dataset of 14 and 90 days,
280 respectively.

281 For the synthetic dataset, the comparison between methods had to consider the error of each. For this purpose, the
282 metric presented in Belis et al. (2015), the uncertainty-normalised Root Mean Squared Error (RMSE_u) was used:

$$283 \quad RMSE_u = \frac{\sqrt{\frac{1}{n} \sum_{i=1}^n (m_i - r_i)^2}}{2u} \quad (7)$$

284 In this expression, m represents the modelled values, r the reference values and u the mean uncertainty of the
285 model.

286 3 Results and discussion

287 3.1 Synthetic dataset

288 This section aims to assess the quality of the outcome of the *rolling* and *seasonal* PMF methods. Relying on
289 synthetic ToF-ACSM data offers the opportunity to compare the PMF outputs to the truth which is not available
290 for real-world measurements. We focus here on the OA sources' (factors') mean concentration and their temporal
291 variability as well as the mean chemical composition and their temporal variability.

292 Regarding the OA apportionment vs. the input OA scatterplot, Table S4 presents the fitting coefficients for several
293 resolutions with no substantial difference between methods. Figure 1 shows the relative factor contributions to the
294 apportioned OA for both methods. The POA factors do not differ substantially between the SA methods, but they
295 are underestimated **with respect to the truth**, (25% of OA in *rolling* and *seasonal*, 35% in truth). Also, whilst the
296 LO-OOA-to-MO-OOA ratio is nearly one in the *rolling* case, it presents a much fresher secondary aerosol for the
297 *seasonal* (1.5). Compared to the *truth*, PMF using a priori information on POA's chemical composition (HOA,
298 BBOA) underestimates POA and overestimates SOA.

299 Figure 2 presents the time series, diel cycles of the truth, and *rolling* and *seasonal* methods, as well as the, scatter
300 plots between the corresponding PMF time series. In time series and diel plots, it is noticeable that SOA is
301 overestimated by PMF at the expense of POA (Fig. 2(c)). Squared Pearson correlation coefficients and slopes were
302 similar for both *rolling* and *seasonal*, respectively, for HOA (0.89,0.88) and OOA (0.95, 0.97), but not for BBOA
303 which *seasonal* resolves better (0.55,0.72). Welch's t-tests between *rolling* and *seasonal* time series rejected the
304 similarity of all factors' concentrations. This test applied to both methods against the truth also rejected the
305 hypothesis of significantly similar means, discarding a good method representation of truth results. This could be
306 explained by the fact that truth profiles are static and the methods were trying to adjust to moving fingerprints and
307 the anchor profiles might have influenced the results. The uncertainty-biased RMSE (RMSE_u, equation (7)) values
308 are 1.10, 0.90 for HOA, 0.95, 1.98 for BBOA and 0.05 and 0.33 for SOA, respectively for *rolling* and *seasonal*
309 PMF results. Values under one represent values within the range of PMF uncertainty, and therefore acceptable
310 values, all in this case except for *rolling* HOA and *seasonal* BBOA. These exclusions could be explained by two

Eliminado: concerning

312 non-exclusive hypotheses: i. The dissimilarity between methods and truth is large; ii. The uncertainties of the
313 methods might be underestimated. In all cases except for HOA, *seasonal* presents higher RMSEu and therefore a
314 worse fit to the truth. Besides, the statistical Welch's t-test was performed on the synthetic dataset PMF results,
315 testing the null hypothesis of statistically similar means with different variances.

316 The difference in Pearson squared correlation coefficients between factors and their potential markers is shown as
317 a histogram in Figure S1 for each of the methods. The truth results show the worst correlation with ancillary
318 measurements compared to modelled PMF. *Rolling* and *seasonal* results are very similar, although these
319 correlations seem greater for *rolling* POA factors and for *seasonal* SOA factors. Slightly higher correlation
320 coefficients were found for *rolling* in transition periods (i.e., ± 7 days before/after the change of seasons) for the
321 *rolling*: 0.88 and 0.77 for HOA vs. BC, 0.74 and 0.65 for HOA vs. NO_x, 0.52 and 0.52 for OOA vs. NH₄ and 0.07
322 and 0.07 for MO-OOA vs. SO₄.

323 Profiles (Figure 3(a)) did not show remarkable discrepancies between PMF methods, but these could be
324 nonetheless noticed when compared to the truth profiles. The cosine similarity method, though, revealed high
325 similarity from both methods to synthetic profiles (1.00 and 1.00 for HOA, 0.91 and 0.91 for BBOA and 1.00 and
326 1.00 for SOA for *rolling* and *seasonal* PMF, respectively). However, it is noteworthy that both HOA's and
327 BBOA's chemical compositions were constrained. Model HOA profiles were very similar to the truth, except for
328 the lower m/z 44 and higher m/z 57 of truth, and other HOA markers regarding models. Modelled BBOA presented
329 significant differences from the truth to modelled profiles, the truth profiles contained a lower m/z 44-to-m/z 43
330 ratio, the lower influence of HOA markers and a much higher m/z 60 and m/z 73, BBOA tracers. Hence, modelled
331 BBOA contained a higher proportion of other OA factor markers and lower of their own, meaning modelled
332 profiles might have resulted in less clean than the true ones. SOA PMF modelled profiles contained lower m/z 43
333 and m/z 44 than the truth profiles, although the rest remains very alike. In short, PMF results present a BBOA
334 factor with more SOA and HOA influence as the main profile. The underestimation of POA is therefore understood
335 due to a poorer modelization of the key source identifiers, leading to a less pure profile and hence, a lower mass
336 apportionment compared to truth.

337 The influence of reference profile constraints might have enhanced the misattribution of the profiles, for example,
338 imposing m/z44-to-m/z43 ratios has led to a significant difference in the degree of oxidation solution with respect
339 to truth. Nevertheless, constraining profiles has provided more accurate solutions than unconstrained set-ups, as
340 shown in Figure S2. These plots show how *seasonal* constrained PMF launches always present higher similarity
341 to *truth* in terms of key ions ratios. Moreover, OA sources of unanchored runs were less robust due to lower
342 reproducibility along accumulation of runs. By extension, *rolling* results are expected to reproduce the same results
343 as it has been proven that both techniques' outcomes converge sufficiently.

344 The adaptability of the models can be assessed from Figure 3 (b), where the 60/55 vs. 44/43 (which are proxies
345 for the BBOA-HOA differentiation and the SOA oxidation, respectively) is plotted for the truth and both methods.
346 Here we use m/z 55 since it is known to be a key marker for HOA. *Rolling* is shown to be as a continuous time
347 series, as the profiles for this method are time-dependent, whilst these ratios for *seasonal* only vary from season
348 to season. In HOA, the modelled points circle the actual truth and anchor profile points (which are similar or

Eliminado: concerning

Eliminado:

Con formato: Fuente: Cursiva

Con formato: Fuente: Cursiva

Eliminado: m/z

equal), but this is not the case for BBOA, in which the *rolling* and *seasonal* points are near the anchor profile but distant from the truth. This implies that the anchor profile, which was selected ignoring the truth profile characteristics, plays an important role in terms of adaptability to the actual solution. Overall, even for OA sources with nominally constant chemical composition (here HOA, BBOA), the factors resolved by PMF exhibit a varying chemical composition. Therefore, caution is required in interpreting the variability in sources of chemical variability resolved by rolling PMF. Oppositely, the SOA profiles, as they were unconstrained, can be compared more fairly. Both the *rolling* and *seasonal* dots are within the truth markers except for some points of high 60/55 for which the highest disparity to truth is found for *seasonal*. This is suggesting a poorer PMF OOAs chemical composition profile apportionment, which in turn, might be influenced by the POA anchoring deficiencies.

The benefits of the continuity of the *rolling* profiles are reflected in time series as can be seen in Figure 3 (c), in which the behaviour of *seasonal* points is unrealistically drastic depending on the season. The profile adaptability of the *rolling* method represents a more resolute approach to positively representing the truth. Contrarily, the *seasonal* approach, although can be plotted for each timestamp as SOA is the sum of two OOAs, can only vary in lines of equal 44/43 ratio as the profiles are constant all over a season. In short, it can be stated that as opposed to *seasonal* PMF or in general batch-wise PMF analysis, *rolling* PMF offers the potential to interpret changes (e.g. seasonal) in OA sources' chemical composition, but the anchor profile selection has been shown to generate significant discrepancies to the truth for both methods requiring caution in interpreting such variability.

The SA method used has a severe impact on model scaled residuals. Figure S3(a) shows the histogram of the scaled residuals for all the resolutions. In all cases, the *rolling* PMF histogram is significantly sharper, more centred to zero. Also, the same effect is visible in the transition periods (Figure S3(b)). Regarding Q values, the *rolling* value (3838356) is lower than the *seasonal* value (24665377), as expected due to a higher extent of degrees of freedom of the former method. Q/Q_{exp} values, computed from equations (5) and (6), are 7.08 and 37.58, respectively for *rolling* and *seasonal* PMF. The fact that normalising by the model-specific degrees of freedom the Q/Q_{exp} is lower for *rolling* than for *seasonal* leads to the conclusion that the minimization of uncertainty-weighted errors is better achieved by the *rolling* method.

Eliminado: S2

Eliminado: S2

3.2 Multi-site comparison

3.2.1 Preliminary tests

Preliminary tests were performed to check the consistency of the reported results as well as the actual difference between the methods reported. An important performance metric is the closure of the OA mass, that is to say, the difference between the sum of all OA factors concentrations vs. the input mass. Table S4 provides the fit statistics of the input OA vs. the outcome OA for all the sites and four different time spans for the whole period, a season, a fortnight and a day. All squared correlation coefficients are higher than 0.88, and slopes are within the 0.92-1.09 range. This ensures the quality of the PMF performance at all time resolutions and for both methods. A closer inspection of the table shows slightly higher correlation coefficients and slopes closer to one for *rolling*.

388 In order to confirm or reject the existence of systematic disparity between both methods, a two-tailed Welch's t-
 389 test was performed under the null hypothesis of the time series having statistically similar expected values. In
 390 Table S5, all cells marked represent the runs that reject the null hypothesis i.e., for which the factors retrieved from
 391 *rolling* and *seasonal* are not statistically equal (p-values over 0.05). The row 'all' refers to the concatenation of all
 392 the dataset time series. Apportioned OA presents the highest acceptance of the hypothesis rate, implying that the
 393 global apportionment means are not significantly different. The factors with higher rejection rates are LO-OOA,
 394 MO-OOA and HOA and in this order. OOA factors, as they are unconstrained, might be rather sensitive to source
 395 outbreaks or variations, which can have been caught or not by one model, although their sum (OOA) remains
 396 coherent. Period-long figures get the highest rejection rates, which decay rapidly from lower to higher resolutions,
 397 meaning the seasonal and fortnightly averages are still high despite their rapid resolution while for the daily
 398 resolution this rate is very low. This fact highlights that the methods yet present significant differences in means
 399 in intermediate resolutions.

400 Figure S4 compares the relative difference of the *rolling* minus *seasonal* concentrations for each factor in the all-
 401 sites ensemble. The factors with higher errors are MO-OOA, LO-OOA, tilted to positive values, this is, resulting
 402 in higher concentrations for *rolling*. This is probably related to the lack of anchors which promotes higher freedom
 403 and hence, higher difference between methods. Also, BBOA presents significant positive whiskers, but as mean
 404 concentrations in Figure 1 are equal, we suspect these are linked to sporadic high concentration outbreaks, which
 405 might only have been caught by the *rolling* method. Besides, the other factors are not significantly different from
 406 zero.

Eliminado: S3

407 The pie charts in Figure 4 show the amount of mass apportioned by the main OA sources in all datasets. These
 408 pies do not account for site-specific sources, they present the relative contribution of the all-sites ones scaled to
 409 account for the 360 degrees. OA is mainly driven by secondary organic aerosols in both cases, although the ratio
 410 of fresh-to-aged aerosol contribution, that is, LO-OOA over MO-OOA, is much higher for *rolling* (0.62) rather
 411 than for *seasonal* (0.54). The ratio POA over SOA is higher for *seasonal* than for *rolling* (0.58 and 0.37,
 412 respectively), and the ratio BBOA over HOA is considerably different (1.17 and 1.45, respectively). The fact that
 413 wood burning exceeds fossil fuel is consistent with the average ratio for BC_{wb} and BC_{ff} of 3.1, implying that PMF
 414 reproduces this relation. Hence, *rolling* describes a more oxidised SOA, which is less prevailing than that from
 415 *seasonal*. In both, POA is governed by the biomass burning OA. Figure S5 shows the individual apportionment
 416 pies, in which the same trends can be generally recognized. In general terms, these results do not coincide with the
 417 synthetic dataset ones, in which the POA/SOA and LO-OOA / MO-OOA ratios were, respectively, equal and
 418 higher for *rolling*.

Eliminado: S4

419 Figure 5 shows both the monthly and diel cycles of *rolling* minus *seasonal* concentrations of the ensemble of sites
 420 for the main factors. In general terms, the intra-year variation is not remarkable as mainly all the boxes are crossing
 421 the zero line. Besides, the differences between mean and median could indicate the adaptability to spiky events.
 422 The fact that HOA and BBOA are remarkably different throughout the whole period coincides with Welch's t-tests
 423 aforementioned. Moreover, the mean for HOA in January and December and for BBOA in July and August are
 424 positively set beyond the boxes, which could imply that the most extreme events are better captured by the *rolling*.
 425 This fact reinforces the hypothesis of a more precise capture of intra-month events. SOA factors present fewer

428 clear trends, although an alternate sign between warm and cold months can be recognised. Figure S6 depicts the
429 behaviour of the remaining factors, which are nearly zero except for 58-OA, which is significantly negative in
430 summer and SHINDOA, which alternates from positive to negative from summer to winter. In the case of 58-OA,
431 this indicates a summertime under/overestimation of one of the methods, and for the SHINDOA, a differing
432 capturability of events along the year.

Eliminado: 5

433 Regarding diel cycles (Figure 5), the differences are evident in HOA and BBOA at night, implying there is where
434 the mixing between POA sources is aggravated. The SOA factors reveal one of the methods overestimates the
435 other throughout the daily cycle: *rolling* is greater for MO-OOA and OOA and lower for LO-OOA. Whilst these
436 differences do not have an impact on the Welch's t-test for LO-OOA, they do for the rest, even for HOA for which
437 they are not very uneven, probably due to compensation of differences while averaging. Figure S6 shows similar
438 behaviour for both methods in all the factors except for the WCOA, PCOA, CCOA, which present higher
439 differences at night. *Seasonal* concentrations, though, are remarkably higher for 58-OA throughout the period/daily
440 cycle, a bit superior in the COA 8h peak and inferior in the SHINDOA afternoon. While these results do not have
441 an impact on the p-value for the Barcelona - Palau Reial and Magadino sites, it does for the Marseille-Longchamp
442 site.

Eliminado: S5

443 3.2.2 PMF goodness evaluation

444 3.2.2.1 Correlation with ancillary measurements

445 In order to assess the quality of each PMF method outcome, the correlation of factors with their potential markers
446 was monitored from a single and global perspective. The pairs of variables compared were: HOA and BC_{fr} , HOA
447 and NO_x , BBOA and BC_{wb} , MO-OOA and SO_4^{2-} , OOA and NH_4^+ . SHINDOA was compared to ultrafine particles
448 of diameters 10 - 20 nm coming from shipping/industry, differentiated according to Chazeau et al. (2021),
449 Rodríguez and Cuevas, (2007). The correlation of LO-OOA vs. NO_3^- has been excluded in this study due to the
450 plentiful sources of NO_3^- ; besides organonitrates would hamper the traceability of LO-OOA from this compound.
451 This analysis has not been extended for the rest of the OA sources due to the lack of appropriate tracers available.

452 Figure 6 presents the Pearson-squared correlation coefficient for all the pairs of markers and factors retrieved from
453 *rolling* and *seasonal* PMF. Even though these marker time series are not deprived of errors, the hypothesis is that
454 better agreement leads to better adaptation of the model to the OA source emitting these tracers. Overall, the *rolling*
455 boxes are centred to higher correlation values than the *seasonal* ones but their whiskers always reach the maximum
456 value of one in both cases. The difference between methods is small since medians do not differ more than 0.05,
457 however, the *seasonal* performance is slightly underscoring these correlations. This finding would support the
458 hypothesis of the superior performance of the *rolling*, although HOA is evenly characterised in both methods,
459 which is consistent with the great similarity in the apportionment of OA shown in Figure 4. The histogram for the
460 difference of Pearson-squared correlation coefficients is plotted as a histogram for all sites in Figure S7. Positivity
461 in this graph reflects better *rolling* results matched with co-located measurements, and the histogram spreads the
462 range of correlations. The amount of shoulders in the right half of these histograms is higher than those in the left,

Eliminado: S6

466 which implies systematic improvement of the *rolling* method with respect to *seasonal* in terms of correlation with
467 ancillary measurements.

468 Periods of transition from one season to another are strategically relevant for this comparison since the *seasonal*
469 method, due to its profile staticity definition, could yield to discontinuities in the time series of the different
470 components. The change of OA factors spectra for *rolling* is smooth, therefore no abrupt changes should be
471 expected in the season edges. Moreover, the *rolling* technique is capable of introducing factors depending on
472 criteria compliance, therefore, their concentration edges are not as sharp as they would be for the *seasonal* PMF.
473 This is the case for BBOA appearance in the cold months in Barcelona - Palau Reial and Marseille - Longchamp,
474 and the 58-OA outbreak after Q-ACSM filament replacement in Magadino. From these premises, one could expect
475 to find better correlation coefficients relating to factors and their markers for the *rolling* method, which could
476 better represent these periods. Table S6 shows the correlation of the OA factors and their markers only for these
477 periods both for the *rolling* and *seasonal* PMF. In all cases, the differences between methods are not extensive.
478 However, it can be seen how the ‘whole’ dataset figures are always greater for *rolling* rather than for *seasonal*.
479 This finding supports the conjecture that the *seasonal* method presents greater difficulty representing the edges of
480 the seasons. The relevance of this conclusion is to be considered especially in the datasets in which the number of
481 days near season changes is important due to data gaps.

482 3.2.2.2 Model residuals

483 Figure 7 shows the normalised scaled residuals distribution for both methods in a concatenated dataset including
484 all the sites. Given that the uncertainty matrix was the same for both techniques, scaled residuals reflect the
485 capacity of each technique to apportion the most similar quantity of OA as was entered as input. Boxplots show a
486 tendency towards negative values for both methods, implying a systematic bias towards the overestimation of the
487 input matrices. *Seasonal* errors present a higher spread and lower mean and medians; hence, *seasonal* results are
488 less accurate and precise than those from *rolling*, overall. However, the span of both distributions does not exceed
489 the $\pm 3\sigma$ threshold in any of the cases, meaning the results are acceptable for both techniques. Figure S8 shows the
490 same plot for each of the participant sites. In general, the *rolling* histograms are more centred to zero and their
491 sharpness is higher with respect to *seasonal* distributions. An exception to this behaviour is Marseille –
492 Longchamp, which presents negatively-shifted distributions probably related to the model’s difficulty to
493 differentiate between BBOA and LO-OOA.

Eliminado: S7

494 Scaled residuals for the season transition periods are presented in Figure S9. Both histograms extend largely
495 beyond the (-3, 3) domain, implying both methods struggle in this kind of period, but the *seasonal* distribution of
496 scaled residuals is much wider than that of *rolling*. Also, in the zoomed (-3, 3) range, *seasonal* results seem to
497 present a wider distribution. Distribution shoulders are present in both, negative in *rolling* and positive in *seasonal*,
498 respectively, indicating *rolling* overestimation and *seasonal* underestimation of input concentrations. These
499 findings would imply that even if the methods provide a substantial error in the transition periods, the *rolling* better
500 captures the season change due to its profile adaptability.

Eliminado: S8

501 Regarding Q values, the differences between techniques are presented in Table 2. Unweighted Q values show a
502 clear pattern on lower values for *rolling* PMF except for one site. The SIRT datasets were treated by two different

505 users, which might have led to different PMF steps and unreliable result. The generally greater minimisation of Q
506 performed by the *rolling* PMF method can be explained by the major quantity of runs performed compared to
507 *seasonal* PMF because of the proper definition of the method. Depriving the Q of the degrees of freedom effect as
508 shown in equations (5), (6), the minimisation of both methods is signified. The trend generally points to lower
509 figures for the *rolling* method, but whilst the Q minimization of the unweighted Q was an expected fact, the implicit
510 error reduction cannot be ensured within a theoretical frame. However, the majority of sites (excluding the
511 aforementioned SIRTAs) show lower Q/Q_{exp} values for the *rolling* method.

512 3.2.2.3 Adaptability tests

513 Adaptation tests were designed to inspect how much the methods comply with the input data. One of the main
514 concerns to assess is the adaptability of the output profiles to short-lifetime events (order of magnitude of days),
515 as it is the hypothesis onto which the *rolling* PMF is based. For this purpose, the check was based on the difference
516 between main ion ratios, calculated from input values and the apportioned amounts of these ions by OOA factor
517 profiles for both methods, e.g. $(m/z44 / m/z43)_{input} - OOA (m/z44 / m/z43)_{Rolling or Seasonal}$. This can be seen
518 in Figure S10 in a time-series form for each site. Because $m/z44$ and $m/z43$ are also part of POA profiles, one
519 should not expect to find there a perfect match between the raw and the OOA profiles ratios, but a qualitative idea
520 of how well the profiles adapt to the degree of aerosol ageing. In these plots, generally the *rolling* profile variation
521 seems to adapt better rather than *seasonal*, which is a straight line along a season. Under the same logic, Figure 8
522 shows the site histograms of the $(m/z44 / m/z43)_{input} - OOA (m/z44 / m/z43)_{Rolling or Seasonal}$ values only for
523 periods around the change of season, which have been proven to be tricky for the PMF model.

524 Figure S9 shows in general terms how the *rolling* adapts to the main 44-to-43 trends, whilst *seasonal* can only
525 present a single value for a whole season. Even though the *rolling/seasonal* SOA and the input time series are not
526 expected to match perfectly, the main features of the variability are usually caught by the *rolling*. By taking a look
527 only at the transition periods in Figure 8, the tendency is that the difference between the input ratio and the *rolling*
528 ratio is closer to zero or sharper around it than with *seasonal*. These qualitative appreciations bolster the
529 aforementioned conclusion that *rolling* is adapting the SOA profiles to specific singularities of the input time
530 series, generating thus a more accurate solution.

531 4 Conclusions

532 The present study aimed at performing a comprehensive comparison between the two methodologies of fine
533 organic aerosol (OA) source apportionment through the Positive Matrix Factorization (PMF) model: *rolling* and
534 *seasonal* PMF.

535 The synthetic dataset *rolling* and *seasonal* outputs assessment has been rather fruitful for this comparison. The
536 main highlight of this approach is that the modelled sources could be compared to the ‘truth’ ones, this is the
537 artificially chosen OA sources during the dataset tailoring. Contrasting PMF results against the *truth* highlighted
538 the model overestimation of SOA and underestimation of POA (here in case of using a priori information on
539 POA’s chemical composition) for both *rolling* and *seasonal* and different degrees of SOA oxidation between

Eliminado: 9

Eliminado: S8

methods. Nevertheless, the correlation of *rolling* and *seasonal* with the *truth* time series and profiles show very similar results in terms of concentrations. The temporal variability of OA sources' chemical composition has been shown to oscillate even for POA components with temporally invariant chemical composition and to be severely impacted by the selection of the profile anchors, as it differed significantly from the truth results when the anchor was significantly different to the truth profile. However, the use of profile constraints still provided solution closer to the truth than unconstrained PMF. Besides, the *rolling* method has been proven to give a more sensitive representation of the continuous OA fingerprints variation. Scaled residuals minimisation also supported that the *rolling* solution was mathematically superior to *seasonal*.

The following multi-site comparison pretends to contrast both PMF methods in real-world datasets treated homogeneously under Chen et al. (2022) protocol to observe general performance trends. The *rolling* method generally presents a comparatively similar proportion of Primary OA (POA), and a secondary OA (SOA) of lower oxygenation degree, i.e. the ageing state. The double-tailed Welch's t-test showed that the narrower the window of inspection, the higher the differences between factors retrieved from one method to the other. Moreover, towards weekly or daily periods, SOA factors differ more than POA factors. This fact is likely due to the absence of constraints for the SOA factors during PMF. Contrastingly, POA factors are more dissimilar period-wise. The ratio of BBOA-to-HOA differs considerably from *rolling* to *seasonal* (1.45, 1.17, respectively) for the ensemble of sites, but in any case, it is over 1, as the ratio of BC_{wb} -to- BC_{fit} suggests.

In general terms, *rolling* results correlate better with ancillary measurements than those from *seasonal* for almost each of the considered external datasets at all sites. This is particularly true in the days surrounding the change of season, in which the *seasonal* profiles change drastically from one time point to the following. Model residuals also point to a better minimisation for the *rolling* PMF, although regarding scaled residuals both methods comply with the (-3, 3) range advised by the protocol. The time series of key ions also quantitatively pointed to a better adequation of the *rolling* SOA profiles to the oxygenated OA key ions. Finally, the errors also proved to be more stable for the *rolling* method, while it should be noted that the individual sites' discrepancies from the overall trends have not been discussed in this study.

Overall, these results confirm the hypothesis that the *rolling* PMF can be considered more accurate and precise, globally, than the *seasonal* one, although both meet the standards of quality required by the source apportionment protocol. Moreover, the *rolling* method was already recognised to involve less user subjectivity and computational time as well as to be more suitable for long-term and evolving SA analysis, such as semi-automated online SA. This study, therefore, promotes the acceptance of this novel *rolling* method as an improved approach suitable for source apportionment studies. An additional conclusion stemming from this comparison is that the selection of anchor profiles is highly influencing the OA factors, so local reference profiles are encouraged to minimise this impact.

5 References

Amato, F., Alastuey, A., Karanasiou, A., Lucarelli, F., Nava, S., Calzolari, G., Severi, M., Becagli, S., Gianelle, V. L., Colombi, C., Alves, C., Custódio, D., Nunes, T., Cerqueira, M., Pio, C., Eleftheriadis, K., Diapouli, E., Reche,

578 C., Minguillón, M. C., Manousakas, M. I., Maggos, T., Vratolis, S., Harrison, R. M. and Querol, X.: AIRUSE-
 579 LIFE+: A harmonized PM speciation and source apportionment in five southern European cities, *Atmos. Chem.*
 580 *Phys.*, 16(5), 3289–3309, doi:10.5194/acp-16-3289-2016, 2016.

581 Belis, C. A., Pernigotti, D., Karagulian, F., Pirovano, G., Larsen, B. R., Gerboles, M. and Hopke, P. K.: A new
 582 methodology to assess the performance and uncertainty of source apportionment models in intercomparison
 583 exercises, *Atmos. Environ.*, 119, 35–44, doi:10.1016/j.atmosenv.2015.08.002, 2015.

584 Bozzetti, C., El Haddad, I., Salameh, D., Daellenbach, K. R., Fermo, P., Gonzalez, R., Minguillón, M. C., Iinuma,
 585 Y., Poulain, L., Elser, M., Müller, E., Slowik, J. G., Jaffrezo, J. L., Baltensperger, U., Marchand, N. and Prévôt,
 586 A. S. H.: Organic aerosol source apportionment by offline-AMS over a full year in Marseille, *Atmos. Chem. Phys.*,
 587 17(13), 8247–8268, doi:10.5194/acp-17-8247-2017, 2017.

588 Canonaco, F., Crippa, M., Slowik, J. G., Baltensperger, U. and Prévôt, A. S. H.: SoFi, an IGOR-based interface
 589 for the efficient use of the generalized multilinear engine (ME-2) for the source apportionment: ME-2 application
 590 to aerosol mass spectrometer data, *Atmos. Meas. Tech.*, 6(12), 3649–3661, doi:10.5194/amt-6-3649-2013, 2013.

591 Canonaco, F., Slowik, J. G., Baltensperger, U. and Prévôt, A. S. H.: Seasonal differences in oxygenated organic
 592 aerosol composition: Implications for emissions sources and factor analysis, *Atmos. Chem. Phys.*, 15(12), 6993–
 593 7002, doi:10.5194/acp-15-6993-2015, 2015.

594 Canonaco, F., Tobler, A., Chen, G., Sosedova, Y., Slowik, J. G., Bozzetti, C., Daellenbach, K. R., El Haddad, I.,
 595 Crippa, M., Huang, R.-J., Furger, M., Baltensperger, U. and Prévôt, A. S. H.: A new method for long-term source
 596 apportionment with time-dependent factor profiles and uncertainty assessment using SoFi Pro: application to 1
 597 year of organic aerosol data, *Atmos. Meas. Tech.*, 14(2), 923–943, doi:10.5194/amt-14-923-2021, 2021.

598 Chazeau, B., Temime-Roussel, B., Gille, G., Mesbah, B., D’Anna, B., Wortham, H. and Marchand, N.:
 599 Measurement report: Fourteen months of real-time characterisation of the submicronic aerosol and its atmospheric
 600 dynamics at the Marseille-Longchamp supersite, *Atmos. Chem. Phys.*, 21(9), 7293–7319, doi:10.5194/acp-21-
 601 7293-2021, 2021.

602 Chen, G., Sosedova, Y., Canonaco, F., Fröhlich, R., Tobler, A., Vlachou, A., Daellenbach, K., Bozzetti, C.,
 603 Hueglin, C., Graf, P., Baltensperger, U., Slowik, J., El Haddad, I. and Prévôt, A.: Time dependent source
 604 apportionment of submicron organic aerosol for a rural site in an alpine valley using a rolling PMF window, *Atmos.*
 605 *Chem. Phys. Discuss.*, (December), 1–52, doi:10.5194/acp-2020-1263, 2020.

606 Chen, G., Sosedova, Y., Canonaco, F., Fröhlich, R., Tobler, A., Vlachou, A., Daellenbach, K., Bozzetti, C.,
 607 Hueglin, C., Graf, P., Baltensperger, U., Slowik, J., El Haddad, I. and Prévôt, A.: Time dependent source
 608 apportionment of submicron organic aerosol for a rural site in an alpine valley using a rolling PMF window, *Atmos.*
 609 *Chem. Phys. Discuss.*, 43, 1–52, doi:10.5194/acp-2020-1263, 2021.

610 Chen, G., Canonaco, F., Tobler, A., Aas, W., Alastuey, A., Atabakhsh, S., Aurela, M., Baltensperger, U.,
 611 Bougiatioti, A. and Joel, F.: European Aerosol Phenomenology - 8: Harmonised Source Apportionment of

612 Organic Aerosol using 22 Year-long ACSM / AMS Datasets, 2022.

613 Chen, J. and Hoek, G.: Long-term exposure to PM and all-cause and cause-specific mortality: A systematic review
614 and meta-analysis, *Environ. Int.*, 143(June), 105974, doi:10.1016/j.envint.2020.105974, 2020.

615 Crippa, M., Decarlo, P. F., Slowik, J. G., Mohr, C., Heringa, M. F., Chirico, R., Poulain, L., Freutel, F., Sciare, J.,
616 Cozic, J., Di Marco, C. F., Elsasser, M., Nicolas, J. B., Marchand, N., Abidi, E., Wiedensohler, A., Drewnick, F.,
617 Schneider, J., Borrmann, S., Nemitz, E., Zimmermann, R., Jaffrezo, J. L., Prévôt, A. S. H. and Baltensperger, U.:
618 Wintertime aerosol chemical composition and source apportionment of the organic fraction in the metropolitan
619 area of Paris, *Atmos. Chem. Phys.*, 13(2), 961–981, doi:10.5194/acp-13-961-2013, 2013.

620 Crippa, M., Canonaco, F., Lanz, V. A., Äijälä, M., Allan, J. D., Carbone, S., Capes, G., Ceburnis, D., Dall'Osto,
621 M., Day, D. A., DeCarlo, P. F., Ehn, M., Eriksson, A., Freney, E., Ruiz, L. H., Hillamo, R., Jimenez, J. L.,
622 Junninen, H., Kiendler-Scharr, A., Kortelainen, A. M., Kulmala, M., Laaksonen, A., Mensah, A. A., Mohr, C.,
623 Nemitz, E., O'Dowd, C., Ovadnevaite, J., Pandis, S. N., Petäjä, T., Poulain, L., Saarikoski, S., Sellegri, K.,
624 Swietlicki, E., Tiitta, P., Worsnop, D. R., Baltensperger, U. and Prévôt, A. S. H.: Organic aerosol components
625 derived from 25 AMS data sets across Europe using a consistent ME-2 based source apportionment approach,
626 *Atmos. Chem. Phys.*, 14(12), 6159–6176, doi:10.5194/acp-14-6159-2014, 2014.

627 Daellenbach, K. R., Uzu, G., Jiang, J., Cassagnes, L. E., Leni, Z., Vlachou, A., Stefenelli, G., Canonaco, F., Weber,
628 S., Segers, A., Kuenen, J. J. P., Schaap, M., Favez, O., Albinet, A., Aksoyoglu, S., Dommen, J., Baltensperger, U.,
629 Geiser, M., El Haddad, I., Jaffrezo, J. L. and Prévôt, A. S. H.: Sources of particulate-matter air pollution and its
630 oxidative potential in Europe, *Nature*, 587(7834), 414–419, doi:10.1038/s41586-020-2902-8, 2020.

631 Efron, B.: Bootstrap Methods: Another Look at the Jackknife, *Ann. Stat.*, 7(1), doi:10.1214/aos/1176344552,
632 1979.

633 Forello, A. C., Bernardoni, V., Calzolari, G., Lucarelli, F., Massabò, D., Nava, S., Pileci, R. E., Prati, P., Valentini,
634 S., Valli, G. and Vecchi, R.: Exploiting multi-wavelength aerosol absorption coefficients in a multi-time source
635 apportionment study to retrieve source-dependent absorption parameters, *Atmos. Chem. Phys. Discuss.*, 1–26,
636 doi:10.5194/acp-2019-123, 2019.

637 Fröhlich, R., Cubison, M. J., Slowik, J. G., Bukowiecki, N., Prévôt, A. S. H., Baltensperger, U., Schneider, J.,
638 Kimmel, J. R., Gonin, M., Rohner, U., Worsnop, D. R. and Jayne, J. T.: The ToF-ACSM: A portable aerosol
639 chemical speciation monitor with TOFMS detection, *Atmos. Meas. Tech.*, 6(11), 3225–3241, doi:10.5194/amt-6-
640 3225-2013, 2013.

641 El Haddad, I., D'Anna, B., Temime-Roussel, B., Nicolas, M., Boreave, A., Favez, O., Voisin, D., Sciare, J.,
642 George, C., Jaffrezo, J. L., Wortham, H. and Marchand, N.: Towards a better understanding of the origins, chemical
643 composition and aging of oxygenated organic aerosols: Case study of a Mediterranean industrialized environment,
644 *Marseille, Atmos. Chem. Phys.*, 13(15), 7875–7894, doi:10.5194/acp-13-7875-2013, 2013.

645 Heikkinen, L., Äijälä, M., Daellenbach, K., Chen, G., Garmash, O., Aliaga, D., Graeffe, F., Rätty, M., Luoma, K.,

646 Aalto, P., Kulmala, M., Petäjä, T., Worsnop, D. and Ehn, M.: Eight years of sub-micrometre organic aerosol
647 composition data from the boreal forest characterized using a machine-learning approach, *Atmos. Chem. Phys.*
648 *Discuss.*, 1–47, doi:10.5194/acp-2020-868, 2020.

649 IPCC: Climate Change 2021: The Physical Science Basis. Contribution of Working Group I to the Sixth
650 Assessment Report of the Intergovernmental Panel on Climate Change [Masson-Delmotte, V., P. Zhai, A. Pirani,
651 S. L. Connors, C. Péan, S. Berger, N. Caud, Y. Chen, Cambridge Univ. Press, (In Press), 3949 [online] Available
652 from: https://www.ipcc.ch/report/ar6/wg1/downloads/report/IPCC_AR6_WGI_Full_Report.pdf, 2021.

653 Jiang, J., Aksoyoglu, S., El-Haddad, I., Ciarelli, G., Denier Van Der Gon, H. A. C., Canonaco, F., Gilardoni, S.,
654 Paglione, M., Minguiñón, M. C., Favez, O., Zhang, Y., Marchand, N., Hao, L., Virtanen, A., Florou, K., O'Dowd,
655 C., Ovadnevaite, J., Baltensperger, U. and Prévôt, A. S. H.: Sources of organic aerosols in Europe: A modeling
656 study using CAMx with modified volatility basis set scheme, *Atmos. Chem. Phys.*, 19(24), 15247–15270,
657 doi:10.5194/acp-19-15247-2019, 2019.

658 Jimenez, J. L., Canagaratna, M. R., Donahue, N. M., Prevot, A. S. H., Zhang, Q., Kroll, J. H., DeCarlo, P. F.,
659 Allan, J. D., Coe, H., Ng, N. L., Aiken, A. C., Docherty, K. S., Ulbrich, I. M., Grieshop, A. P., Robinson, A. L.,
660 Duplissy, J., Smith, J. D., Wilson, K. R., Lanz, V. A., Hueglin, C., Sun, Y. L., Tian, J., Laaksonen, A., Raatikainen,
661 T., Rautiainen, J., Vaattovaara, P., Ehn, M., Kulmala, M., Tomlinson, J. M., Collins, D. R., Cubison, M. J., Dunlea,
662 E. J., Huffman, J. A., Onasch, T. B., Alfarra, M. R., Williams, P. I., Bower, K., Kondo, Y., Schneider, J., Drewnick,
663 F., Borrmann, S., Weimer, S., Demerjian, K., Salcedo, D., Cottrell, L., Griffin, R., Takami, A., Miyoshi, T.,
664 Hatakeyama, S., Shimono, A., Sun, J. Y., Zhang, Y. M., Dzepina, K., Kimmel, J. R., Sueper, D., Jayne, J. T.,
665 Herndon, S. C., Trimborn, A. M., Williams, L. R., Wood, E. C., Middlebrook, A. M., Kolb, C. E., Baltensperger,
666 U. and Worsnop, D. R.: Evolution of organic aerosols in the atmosphere, *Science* (80-.), 326(5959), 1525–1529,
667 doi:10.1126/science.1180353, 2009.

668 Ng, N. L., Herndon, S. C., Trimborn, A., Canagaratna, M. R., Croteau, P. L., Onasch, T. B., Sueper, D., Worsnop,
669 D. R., Zhang, Q., Sun, Y. L. and Jayne, J. T.: An Aerosol Chemical Speciation Monitor (ACSM) for routine
670 monitoring of the composition and mass concentrations of ambient aerosol, *Aerosol Sci. Technol.*, 45(7), 770–
671 784, doi:10.1080/02786826.2011.560211, 2011a.

672 Ng, N. L., Canagaratna, M. R., Jimenez, J. L., Chhabra, P. S., Seinfeld, J. H. and Worsnop, D. R.: Changes in
673 organic aerosol composition with aging inferred from aerosol mass spectra, *Atmos. Chem. Phys.*, 11(13), 6465–
674 6474, doi:10.5194/acp-11-6465-2011, 2011b.

675 Ogulei, D., Hopke, P. K., Zhou, L., Paatero, P., Park, S. S. and Ondov, J. M.: Receptor modeling for multiple time
676 resolved species: The Baltimore supersite, *Atmos. Environ.*, 39(20), 3751–3762,
677 doi:10.1016/j.atmosenv.2005.03.012, 2005.

678 Paatero, P.: The Multilinear Engine—A Table-Driven, Least Squares Program for Solving Multilinear Problems,
679 Including the n-Way Parallel Factor Analysis Model, *J. Comput. Graph. Stat.*, 8(4), 854–888,
680 doi:10.1080/10618600.1999.10474853, 1999.

681 Paatero, P. and Hopke, P. K.: Discarding or downweighting high-noise variables in factor analytic models, *Anal.*
682 *Chim. Acta*, 490(1–2), 277–289, doi:10.1016/S0003-2670(02)01643-4, 2003.

683 Paatero, P. and Tapper, U.: Positive matrix factorization: A non-negative factor model with optimal utilization of
684 error estimates of data values, *Environmetrics*, 5(2), 111–126, doi:10.1002/env.3170050203, 1994.

685 Parworth, C., Fast, J., Mei, F., Shippert, T., Sivaraman, C., Tilp, A., Watson, T. and Zhang, Q.: Long-term
686 measurements of submicrometer aerosol chemistry at the Southern Great Plains (SGP) using an Aerosol Chemical
687 Speciation Monitor (ACSM), *Atmos. Environ.*, 106, 43–55, doi:10.1016/j.atmosenv.2015.01.060, 2015.

688 Rai, P., Furger, M., El Haddad, I., Kumar, V., Wang, L., Singh, A., Dixit, K., Bhattu, D., Petit, J. E., Ganguly, D.,
689 Rastogi, N., Baltensperger, U., Tripathi, S. N., Slowik, J. G. and Prévôt, A. S. H.: Real-time measurement and
690 source apportionment of elements in Delhi's atmosphere, *Sci. Total Environ.*, 742, 140332,
691 doi:10.1016/j.scitotenv.2020.140332, 2020.

692 Rodríguez, S. and Cuevas, E.: The contributions of “minimum primary emissions” and “new particle formation
693 enhancements” to the particle number concentration in urban air, *J. Aerosol Sci.*, 38(12), 1207–1219,
694 doi:10.1016/j.jaerosci.2007.09.001, 2007.

695 Rutherford, J. W., Larson, T. V., Gould, T., Seto, E., Novosselov, I. V. and Posner, J. D.: Source apportionment
696 of environmental combustion sources using excitation emission matrix fluorescence spectroscopy and machine
697 learning, *Atmos. Environ.*, 259(May), 118501, doi:10.1016/j.atmosenv.2021.118501, 2021.

698 Shih, C.-H., Chen, J.-K., Kuo, L.-W., Cho, K.-H., Hsiao, T.-C., Lin, Z.-W., Lin, Y.-S., Kang, J.-H., Lo, Y.-C.,
699 Chuang, K.-J., Cheng, T.-J. and Chuang, H.-C.: Chronic pulmonary exposure to traffic-related fine particulate
700 matter causes brain impairment in adult rats, *Part. Fibre Toxicol.*, 15(1), 1–17, doi:10.1186/s12989-018-0281-1,
701 2018.

702 Sun, Y., Xu, W., Zhang, Q., Jiang, Q., Canonaco, F., Prévôt, A. S. H., Fu, P., Li, J., Jayne, J., Worsnop, D. R. and
703 Wang, Z.: Source apportionment of organic aerosol from 2-year highly time-resolved measurements by an aerosol
704 chemical speciation monitor in Beijing, China, *Atmos. Chem. Phys.*, 18(12), 8469–8489, doi:10.5194/acp-18-
705 8469-2018, 2018.

706 Textor, C., Schulz, M., Guibert, S., Kinne, S., Balkanski, Y., Bauer, S., Berntsen, T., Berglen, T., Boucher, O.,
707 Chin, M., Dentener, F., Diehl, T., Easter, R., Feichter, H., Fillmore, D., Ghan, S., Ginoux, P., Gong, S., Grini, A.,
708 Hendricks, J., Horowitz, L., Huang, P., Isaksen, I., Iversen, T., Kloster, S., Koch, D., Kirkevåg, A., Kristjansson,
709 J. E., Krol, M., Lauer, A., Lamarque, J. F., Liu, X., Montanaro, V., Myhre, G., Penner, J., Pitari, G., Reddy, S.,
710 Seland, Stier, P., Takemura, T. and Tie, X.: Analysis and quantification of the diversities of aerosol life cycles
711 within AeroCom, *Atmos. Chem. Phys.*, 6(7), 1777–1813, doi:10.5194/acp-6-1777-2006, 2006.

712 Tobler, A. K., Canonaco, F., Skiba, A., Styszko, K., Nęcki, J., Slowik, J. G. and Baltensperger, U.: Characterization
713 and source apportionment of PM 1 organic aerosol in Krakow , Poland , , (April), 8299, 2021.

714 Ulbrich, I. M., Canagaratna, M. R., Zhang, Q., Worsnop, D. R. and Jimenez, J. L.: Interpretation of organic
 715 components from Positive Matrix Factorization of aerosol mass spectrometric data, *Atmos. Chem. Phys.*, 9(9),
 716 2891–2918, doi:10.5194/acp-9-2891-2009, 2009.

717 Yang, M., Chu, C., Bloom, M. S., Li, S., Chen, G., Heinrich, J., Markevych, I., Knibbs, L. D., Bowatte, G.,
 718 Dharmage, S. C., Komppula, M., Leskinen, A., Hirvonen, M. R., Roponen, M., Jalava, P., Wang, S. Q., Lin, S.,
 719 Zeng, X. W., Hu, L. W., Liu, K. K., Yang, B. Y., Chen, W., Guo, Y. and Dong, G. H.: Is smaller worse? New
 720 insights about associations of PM₁ and respiratory health in children and adolescents, *Environ. Int.*, 120(August),
 721 516–524, doi:10.1016/j.envint.2018.08.027, 2018.

722 Yin, P., Guo, J., Wang, L., Fan, W., Lu, F., Guo, M., Moreno, S. B. R., Wang, Y., Wang, H., Zhou, M. and Dong,
 723 Z.: Higher Risk of Cardiovascular Disease Associated with Smaller Size-Fractioned Particulate Matter, *Environ.*
 724 *Sci. Technol. Lett.*, 7(2), 95–101, doi:10.1021/acs.estlett.9b00735, 2020.

725 Yuan, B., Shao, M., De Gouw, J., Parrish, D. D., Lu, S., Wang, M., Zeng, L., Zhang, Q., Song, Y., Zhang, J. and
 726 Hu, M.: Volatile organic compounds (VOCs) in urban air: How chemistry affects the interpretation of positive
 727 matrix factorization (PMF) analysis, *J. Geophys. Res. Atmos.*, 117(24), 1–17, doi:10.1029/2012JD018236, 2012.

728 Zhang, Y., Favez, O., Petit, J. E., Canonaco, F., Truong, F., Bonnaire, N., Crenn, V., Amodeo, T., Prévôt, A. S.
 729 H., Sciare, J., Gros, V. and Albinet, A.: Six-year source apportionment of submicron organic aerosols from near-
 730 continuous highly time-resolved measurements at SIRTa (Paris area, France), *Atmos. Chem. Phys.*, 19(23),
 731 14755–14776, doi:10.5194/acp-19-14755-2019, 2019.

732

733 **Acknowledgements.**

734 IDAEA-CSIC is a Centre of Excellence Severo Ochoa (Spanish Ministry of Science and Innovation, Project
 735 CEX2018-000794-S). The authors gratefully acknowledge the Romanian National Air Quality Monitoring
 736 Network (NAQMN, www.calitateair.ro) for providing NO_x data.

737 **Financial support.**

738 This work was supported by COST Action CA16109 COLOSSAL, the Generalitat de Catalunya (grant no.
 739 AGAUR 2017 SGR41), the Spanish Ministry of Science and Innovation 70 through the CAIAC project (grant no.
 740 PID2019- 108990RB-I00), and FEDER funds through EQC2018-004598-P. This work has received funding from
 741 the RI-Urbans project from European Union's Horizon 2020 research and innovation programme under grant
 742 agreement No 101036245. This study was partially supported by the European Union's projects ACTRIS (EU
 743 FP7-262254) and ACTRIS-2 (EU Horizon 2020-654109). This work was supported by a grant of the Romanian
 744 Ministry of Research, Innovation and Digitalization, CNCS - UEFISCDI, project number PN-III-P1-1.1-TE-2019-
 745 0340 and through Program 1- Development of the national research-development system, Subprogram 1.2 -
 746 Institutional performance - Projects to finance the excellent RDI, Contract no. 18PFE/30.12.2021, by Romanian

747 National Core Program contract 18N/2019. IMT Nord Europe acknowledges financial support from the Labex
748 CaPPA project, which is funded by the French National Research Agency (ANR) through the PIA (Programme
749 d'Investissement d'Avenir) under contract ANR-11-LABX-0005-01, and the CLIMIBIO project, both financed
750 by the Regional Council "Hauts-de-France" and the European Regional Development Fund (ERDF). The ATOLL
751 and SIRTAs sites are part of ACTRIS-France facilities and also contribute to the CARA program of the LCSQA
752 funded by the French Ministry of Environment. JS and MP acknowledge funding from the European Union's
753 Horizon 2020 Research and Innovation Programme (under grant agreement no. 856612) and the Cyprus
754 Government. National University of Ireland Galway work was supported by the EPA AEROSOURCE Project
755 (2016-CCRP-MS-31) and AC3 network, the Department of Environment, Climate and Communications. GC and
756 AP has been supported by the European Research Council, H2020 European Research Council (ERA-PLANET
757 (grant no. 689443)) and a COST-related project of the Swiss National Science Foundation, the Schweizerischer
758 Nationalfonds zur Förderung der Wissenschaftlichen Forschung (SAMSAM (grant no. IZCOZ0_177063)). K.R.D
759 acknowledges support by the Swiss National Science Foundation Ambizione grant PZPGP2_201992.

760 Figures and tables

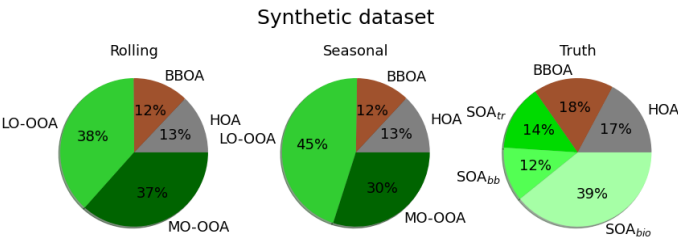
761 **Table 1. Participant sites.**

Site	Type	Latitude	Longitude	Height (m a.s.l.)	ACSM type	Network	Period
Barcelona – Palau Reial (BCN-PR)	Urban background	41° 23' 11.48'' N	02° 07' 05.00'' E	80	Q	ACTRIS, GAW	09/2017 – 10/2018
Cyprus Atm. Obs. - Agia Marina Xyliatou (CAO- AMX)	Remote	35° 2' 19.35'' N	33° 3' 27.95'' E	352	Q	ACTRIS, GAW	03/2015 – 01/2017

Dublin (DUB)	Urban background	53° 18' 19.08'' N	06° 13' 4.52'' W	35	Q	ACTRIS, AQ network in Ireland: http://www.macehead.org/	09/2015 – 08/2017
ATmospheric Observations in liLle (ATOLL)	Suburban	50° 36' 40.0 N	03° 08' 25.4'' E	70	Q	ACTRIS, CARA programme (French AQ network)	10/2016 – 09/2017
Magadino (MGD)	Rural	46°9'37'' N	8° 56' 2'' E	204	Q	GAW	08/2013 – 10/2014
Magurele – INOE (INO)	Peri-urban	44° 20' 52.98'' N	26° 1' 43.93'' E	93	Q	ACTRIS, GAW	09/2016 - 09/2017
Marseille-Longchamp (MRS-LCP)	Urban background	43° 18' 18.84'' N	5° 23' 40.89'' E	71	ToF	CARA programme (French AQ network)	01/2017 – 04/2018
SIRTA (SIR)	Suburban	48° 42' 36'' N	2° 9' 0'' E	163	Q	ACTRIS	01/2016 - 05/2017

Tartu (TAR)	Urban backgroun d	58° 22' 14.16'' N	26° 44' 5.64'' E	39	Q	National Air monitorin g station	09/2016 07/2017	–
----------------	-------------------------	----------------------	---------------------	----	---	---	--------------------	---

762



763

764 **Figure 1. OA apportionment results for rolling ~~and~~ seasonal methods and truth output.**

765

Eliminado: ,

Eliminado:

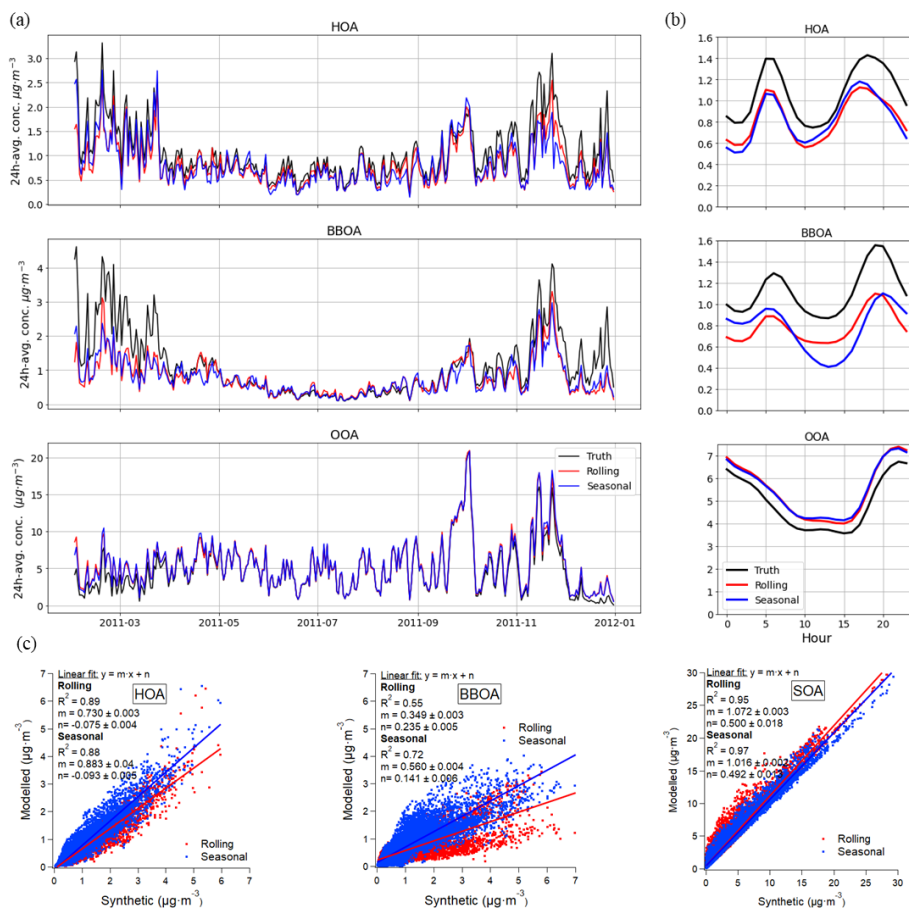


Figure 2. Rolling, seasonal and truth (synthetic dataset original values) (a) time series (in hourly averages for the sake of clarity), (b) diel profiles and (c) scatter plots.

Eliminado: and ,

Eliminado: and (d) factor profiles.

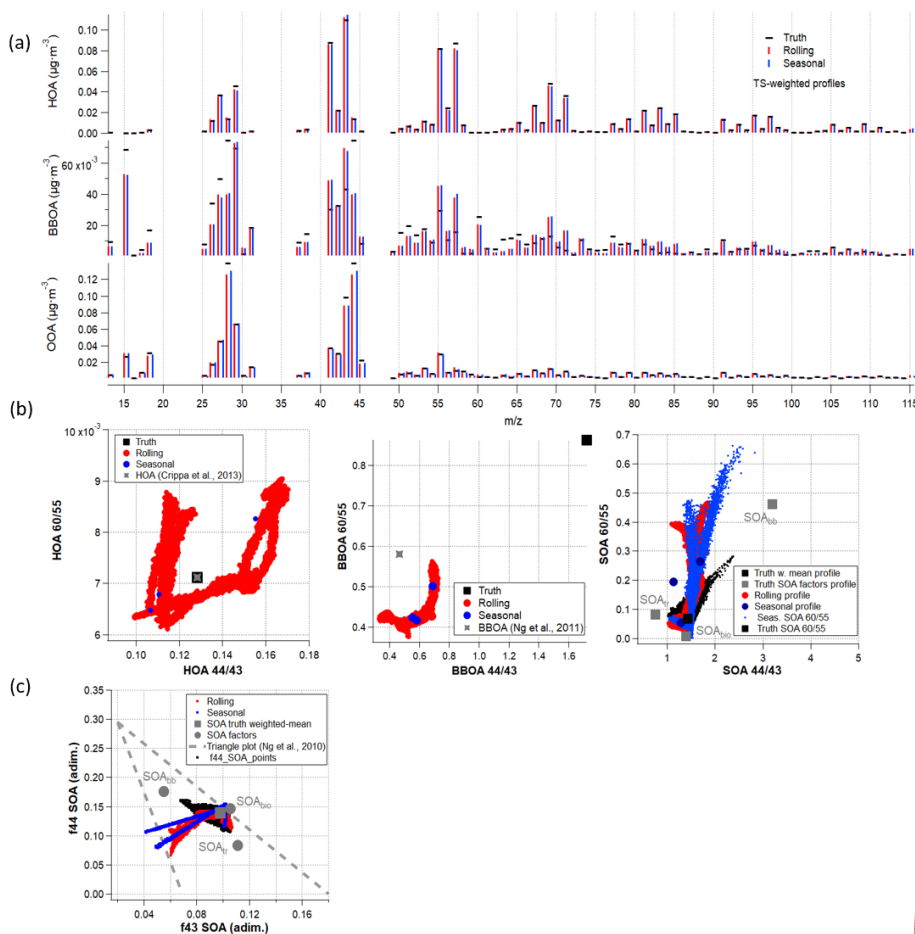
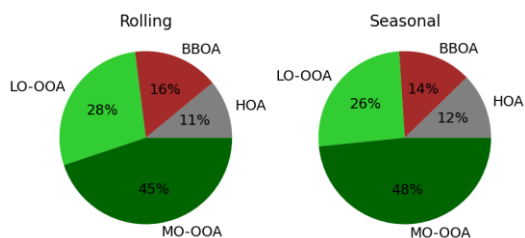
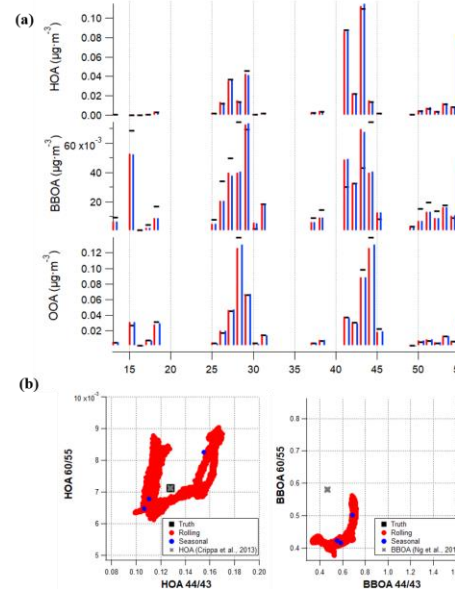


Figure 3. **Synthetic dataset solution** (a) Profiles; (b) Time-dependent profile variability of ratios 60/55 vs. 44/43; (c) Triangle plot of f44 vs. f43; **for rolling PMF (red), seasonal PMF (blue) and truth (black).**



Eliminado: ¶



Con formato: Fuente: Sin Negrita, Color de fuente: Automático

Con formato: Fuente: 10 pto

Eliminado: Main ion ratios for each factor represented as (a) Histograms of the difference with respect to truth of each method.

Eliminado: Synthetic dataset p

Eliminado: of

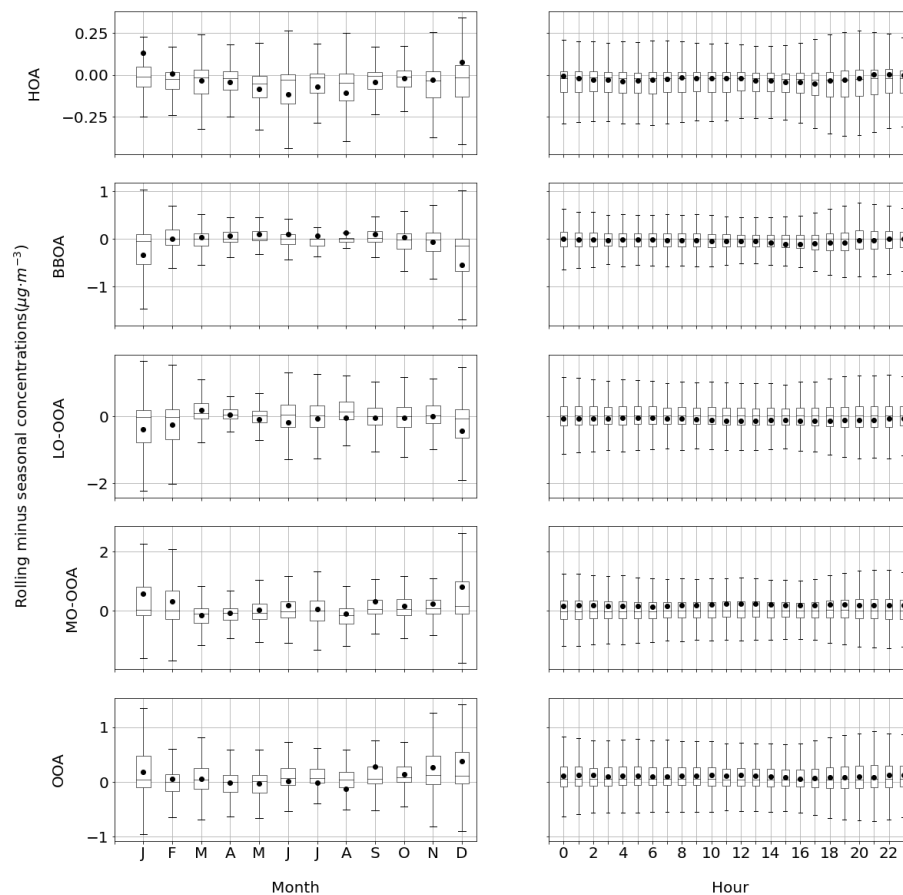
Con formato: Fuente: Sin Cursiva

Con formato: Fuente: Sin Cursiva

Con formato: Fuente: Sin Cursiva

784 Figure 4. Pie charts of the mean concentrations of the main factors for the ensemble of all sites.

Eliminado: all
Eliminado: the



785
786
787 Figure 5. Boxplots of *rolling minus seasonal* factor absolute concentrations (in $\mu\text{g}\cdot\text{m}^{-3}$) per month and hour.
788 Boxes show the Q1-to-Q3 range with the median (horizontal line) and the average (full circles), and whiskers
789 extend up to the range of the data.

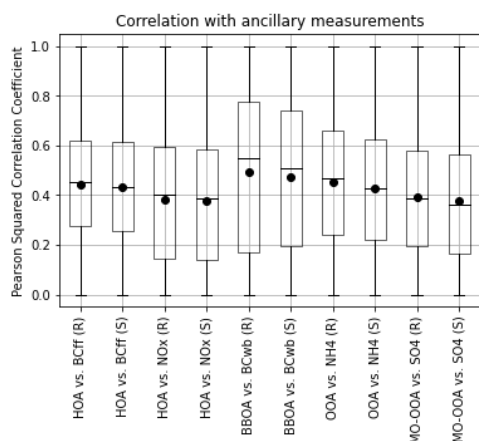


Figure 6. Rolling (R) and seasonal (S) boxplots of the Pearson-squared correlation coefficient of each OA source with its respective markers for all sites.

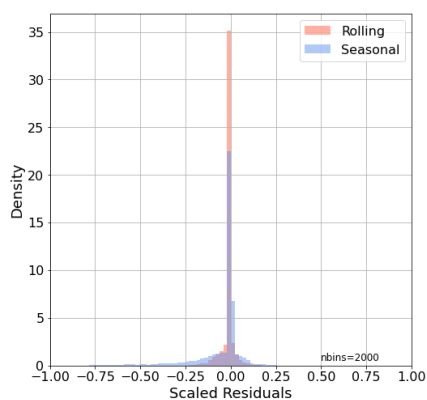


Figure 7. Normalised scaled residuals histogram for both PMF techniques.

Table 2. Q/Qexp values for rolling and seasonal solutions.

Q	Raw		Normalised	
	Rolling	Seasonal	Rolling	Seasonal
BCN - PR	481008	1766588	0.35	1.14
CAO - AMX	57337	5101949	0.04	2.87

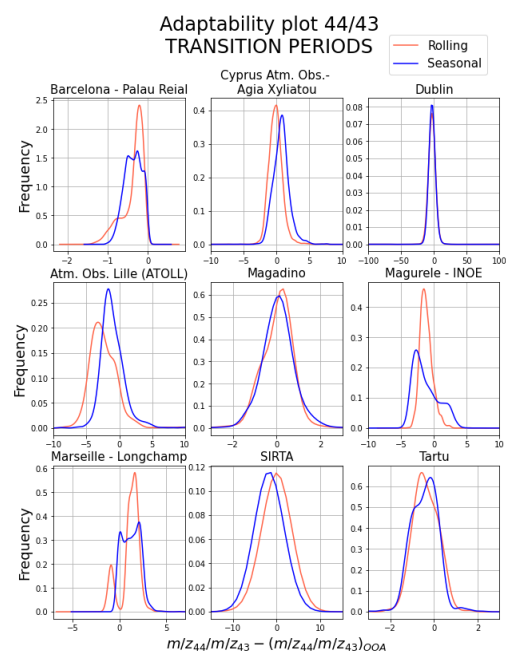
Eliminado: ¶

Con formato: Sin Resaltar

803
804
805
806

DUB	1031616	1261451	1.14	1.19
ATOLL	465480	477145	0.84	0.69
MGD	8463251	3117660	0.75	2.46
INO	6138684	25404272	4.58	17.24
MRS – LCP	57337	5101949	17.24	2.87
SIR	558044	44965	0.47	0.10
TAR	82742	152343	0.59	0.34

807



808 Figure 8. Kernel density estimation of the histograms of the subtraction of the m/z 44-to-43 ratio from the
809 raw (from input matrices) time series data minus the apportioned quantity in profiles. These plots only
810 contain those time lapses among the change of season (transition periods)

Eliminado: both

Eliminado: raw

Eliminado: and

811

812